Supporting Information

Structural Phase Transition and Bandgap Control through Mechanical Deformation in Layered Semiconductors 1T-ZrX_2 (X = S, Se)

Edoardo Martino, David Santos-Cottin, Florian Le Mardelé, Konstantin Semeniuk, Michele Pizzochero, Kristiāns Čerņevičs, Stefan Klotz, Ludovic Delbes, Benoît Baptiste, Francesco Capitani, Helmuth Berger, Oleg V. Yazyev and Ana Akrap**

[1] Institute of Physics, Ecole Polytechnique Fédérale de Lausanne (EPFL), CH-1015 Lausanne, Switzerland

[2] Department of Physics, University of Fribourg, CH-1700 Fribourg, Switzerland

[3] Institut de Minéralogie, de Physique des Matériaux et de Cosmochimie, Sorbonne University, CNRS UMR 7590, IMPMC, F-75005, Paris, France

[4] Synchrotron-SOLEIL, Saint-Aubin, BP48, F-91192 Gif-sur-Yvette Cedex, France

E-mail: edoardo.martino@epfl.ch, ana.akrap@unifr.ch

Crystals synthesis: Single crystals of 1T-ZrS_2 and 1T-$ZrSe_2$ were synthesized by chemical vapour transport method using I_2 as transport agent. Similar conditions as those presented in [37] have been used to grow large single crystals.

High-pressure Raman and infrared spectroscopy: Raman and infrared measurements were performed on the infrared beamline SMIS at the synchrotron SOLEIL. We used a DXR2 Thermo Fisher Raman microspectrometer equipped with a 633nm He-Ne laser as light source, a Peltier cooled CCD detector, a 600 grooves/mm grating, resulting in a spectral resolution of about 4 cm^{-1}. Infrared measurements were performed on a custom-built horizontal microscope for diamond anvil cells (DACs), equipped with custom Cassegrain objectives, a MCT and a Si diode detectors, for the Mid-IR and the Near-IR respectively [1]. The horizontal microscope was coupled to Thermo Fisher iS50 interformeter with Quartz (NIR) / KBr (MIR) beamsplitters and synchrotron radiation as IR source.

Square samples of about 100 × 100 μm^2 were loaded into a membrane DAC with 400 µm culets. Stainless-steel gaskets were pre-indented to a thickness of about 50 µm and a hole of diameter 150 um was drilled by electro-erosion. NaCl was used as pressure transmitting medium [2]. Pressure was measured in situ by the standard ruby fluorescence technique. Data was collected

every 1 GPa during both compression and decompression, with the last data point collected after the cell was open to release any residual pressure.

Sample thickness for optical transmittance experiments was determined before the measurement by means of optical interference, analyzing the oscillations of the transmitted light intensity as a function of wavelength (Fabry Perot interference). For the computation, the refractive index of the materials at energies below the bandgap is n = 4 [3]. The value of the refractive index is experimentally determined through ellipsometry.

X-ray diffraction: The high-pressure X-ray diffraction experiments were performed at the X-ray diffraction platform of IMPMC at 0.85GPa and 293K, using a membrane diamond anvil cell (DAC) with a culet of 500 μm in diameter. A 250 μm-diameter hole was drilled in a stainless-steel gasket with a thickness of 200 μm pre-indented to 80 μm. The finely ground powders of $ZrSe_2$ and ZrS_2 were loaded into the gasket hole together with a ruby ball as pressure sensor [4] (R1 ruby fluorescence method). A 4:1 methanol-ethanol mixture was used as pressure transmitting fluid since it is known to provide hydrostatic conditions to approximately 10 GPa [5]. Before and after each measurement, pressure was determined by recording the ruby fluorescence spectra using a spectrometer with a 532 nm excitation laser. The calculated error for the pressure values is 0.1 GPa and the sensitivity was 0.05GPa.

The DAC was then mounted on a Rigaku MM007HF diffractometer equipped with a Mo rotating anode ($\lambda_{K\alpha1}$ = 0.709319 Å, $\lambda_{K\alpha2}$ = 0.713609 Å), VariMax focusing optics and a RAXIS4++ image plate detector. X-ray data were collected at 20 °C. A LaB_6 standard sample was measured in the same experimental conditions to calibrate the FIT2D program, the image processing software used to integrate the intensities around the Debye−Scherrer rings and to get the 1D patterns.

Density Functional Theory Calculations*:* Our first-principles calculations were performed at the density functional theory level as implemented in VASP [6,7]. We adopted the hybrid HSE06 [8] functional for describing the semiconducting systems, and the semilocal PBE functional for the metallic one [9]. Electron-core interactions were described through the projector augmented wave method, while Kohn-Sham wavefunctions were expanded in a plane wave basis set with a cutoff on kinetic energy of 400 eV. The integration over the Brillouin zone was carried out using a 6×6×4 (6×4×2) k-mesh for the low-pressure (high-pressure) crystalline phase of $ZrSe_2$. We relied on the experimental crystal structures determined in our X-ray diffraction experiments.

High-pressure Rietveld refinement of the XRD spectra

The crystal structure refinements were carried out using the Rietveld method as implemented in the Fullprof software [10].

Starting from the known cell parameters of ZrS_2 and $ZrSe_2$, the refinements converged rapidly for the known structures at low pressure, considering low amounts of iron (diffraction from the DAC gasket).

For the two structures, preferred orientations were evidenced and their relative parameters refined: (001) for 1T-ZrS_2, (-101) for HP-ZrS_2, (001) for 1T-$ZrSe_2$, and (010) for HP-$ZrSe_2$.

The peak widths were significantly larger than the instrument resolution (~0.15° 2θ). Starting from an instrumental resolution function, Lorentzian isotropic size (Y) and Lorentzian isotropic strain (X) parameters were refined but only the second one (strain effect) improved the fits. Then, anisotropic refinements of strain parameters were attempted to get better peak profiles. The corresponding spherical harmonic coefficients are given in the following tables but the estimated standard deviations (esd) are too large to discuss the physical meaning of these values.

The low data to parameter ratio at high pressure - mainly due to the coexistence of starting and HP structure and to the peak broadening increasing with the strain - prevent us from a stable refinement of atomic positions.

Table 1. Results of the Rietveld refinement from X-ray diffraction analysis (λ_{Mo}) of ZrS_2.

Pressure 0.37GPa			
1T-ZrS_2	*P* -3*m1*	R_{Bragg} = 9.93 %	Fract. (%) = 96 (4)
a = b = 3.6619 (11) Å	*c* = 5.7746 (24) Å		
V = 67.059 (40) Å^3			
Strain Parameters (for profile only, large esd)			
S_{400}=3.21 (2.43), S_{004}=11.11 (4.70), S_{112}=0			
Fe	*I m3m*	R_{Bragg} = 11.7 %	Fract. (%) = 4 (1)
a = 2.8771 (52) Å			
V = 23.816 (74) Å^3			
Pressure 2GPa			
1T-ZrS_2	*P* -3*m1*	R_{Bragg} = 16.3 %	Fract. (%) = 93 (4)
a = b = 3.6365 (9) Å	*c* = 5.6330 (19) Å		
V = 64.511 (31) Å^3			
Strain Parameters (for profile only, large esd)			
S_{400}=1.73 (1.96), S_{004}=8.20(+/-3.71), S_{112}=0			
Fe	*I m3m*	R_{Bragg} = 30.2 %	Fract. (%) = 7 (1)
a = 2.8714 (39) Å			
V = 23.675 (56) Å^3			
Pressure 4GPa			
1T-ZrS_2	*P* -3*m1*	R_{Bragg} = 12.1 %	Fract. (%) = 56 (5)
a = b = 3.6122 (7) Å	*c* = 5.5275 (26) Å		
V = 62.461 (34) Å^3			
Strain Parameters (for profile only, large esd)			
S_{400}=1.25 (0), S_{004}=5.67(4.86), S_{112}=0.23 (11.30)			
HP-ZrS_2	*P* 2_1/*m*	R_{Bragg} = 17.8 %	Fract. (%) = 38 (8)
a = 6.4811 (104) Å	*b* = 3.7610 (10) Å	*c* = 5.0823 (126) Å	β= 108.922(50) deg
V = 117.188 (341) Å^3			

Strain Parameters (for profile only, large esd)

S_{400}=45 (83), S_{040}=55(66), S_{004}=140(306), S_{220}=138(127), S_{202}=0

S_{022}=0, S_{121}=-0, S_{301}=0, S_{103}=0

Fe	*I m3m*	R_{Bragg} = 15.0 %	Fract. (%) = 6 (1)
a = 2.8616 (30) Å			
V = 23.433 (42) Å^3			

Pressure 6GPa			
1T-ZrS_2	*P -3m1*	R_{Bragg} = 6.2 %	Fract. (%) = 37 (4)
a = b = 3.5904 (17) Å	*c* = 5.4493 (52) Å		
V = 60.837 (71) Å^3			
Strain Parameters (for profile only, large esd)			
S_{400}=26 (29), S_{004}=0 (8), S_{112}=0			
HP-ZrS_2	*P 2$_1$/m*	R_{Bragg} = 11.6 %	Fract. (%) = 55 (6)
a = 6.4766 (63) Å	*b* = 3.7235 (25) Å	*c* = 4.9906 (75) Å	β= 108.549(54) deg
V = 114.100 (218) Å^3			
Strain Parameters (for profile only, large esd)			
S_{400}=45 (28), S_{040}=146(52), S_{004}=46(60), S_{220}=88(90), S_{202}=124 (104)			
S_{022}=0, S_{121}=-0, S_{301}=0, S_{103}=0			
Fe	*I m3m*	R_{Bragg} = 7.1 %	Fract. (%) = 8 (1)
a = 2.8587 (34) Å			
V = 23.363 (48) Å^3			
Pressure 8GPa			
1T-ZrS_2	*P -3m1*	R_{Bragg} = 8.7 %	Fract. (%) = 28 (6)
a = b = 3.5789 (28) Å	*c* = 5.4162 (99) Å		
V = 60.081 (128) Å^3			
Strain Parameters (for profile only, large esd)			
S_{400}=109 (85), S_{004}=63 (69), S_{112}=126 (138)			
HP-ZrS_2	*P 2$_1$/m*	R_{Bragg} = 15.0 %	Fract. (%) = 62 (8)
a = 6.4791 (80) Å	*b* = 3.7064 (41) Å	*c* = 5.0004 (123) Å	β= 108.88(11) deg
V = 113.620 (337) Å^3			

Strain Parameters (for profile only, large esd)

S_{400}=64 (26), S_{040}=169 (65), S_{004}=262 (126), S_{220}=162 (109), S_{202}=0

S_{022}=0, S_{121}=-0, S_{301}=0, S_{103}=0

Fe	*I m3m*	R_{Bragg} = 10.1 %	Fract. (%) = 10 (1)
a = 2.8641 (29) Å			
V = 23.493 (41) Å^3			
Pressure 10GPa			
1T-ZrS_2	*P -3m1*	R_{Bragg} = 12.3 %	Fract. (%) = 28 (11)
a = b = 3.5563 (14) Å	*c* = 5.3731 (90) Å		
V = 58.850 (104) Å^3			
Strain Parameters (for profile only, large esd)			
S_{400}=155 (172), S_{004}= 383 (299), S_{112}= 0			
HP-ZrS_2	*P 2$_1$/m*	R_{Bragg} = 15.6 %	Fract. (%) = 65 (9)
a = 6.4673 (94) Å	*b* = 3.6731 (21) Å	*c* = 4.9983 (138) Å	β= 109.23(13) deg
V = 112.106 (355) Å^3			
Strain Parameters (for profile only, large esd)			
S_{400}=11 (22), S_{040}=200 (64), S_{004}=125 (118), S_{220}=210 (85), S_{202}= 286 (134)			
S_{022}=0, S_{121}=-0, S_{301}=0, S_{103}=0			
Fe	*I m3m*	R_{Bragg} = 8.9 %	Fract. (%) = 7.1 (2)
a = 2.8558 (31) Å			
V = 23.290 (44) Å^3			

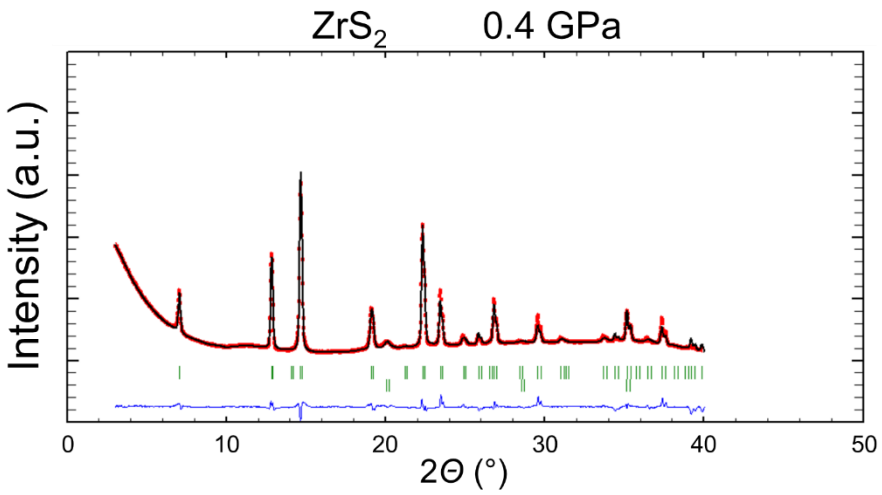
ZrS2 0.4 GPa
Intensity (a.u.)
0
10
20
30
40
50
2Θ (°)

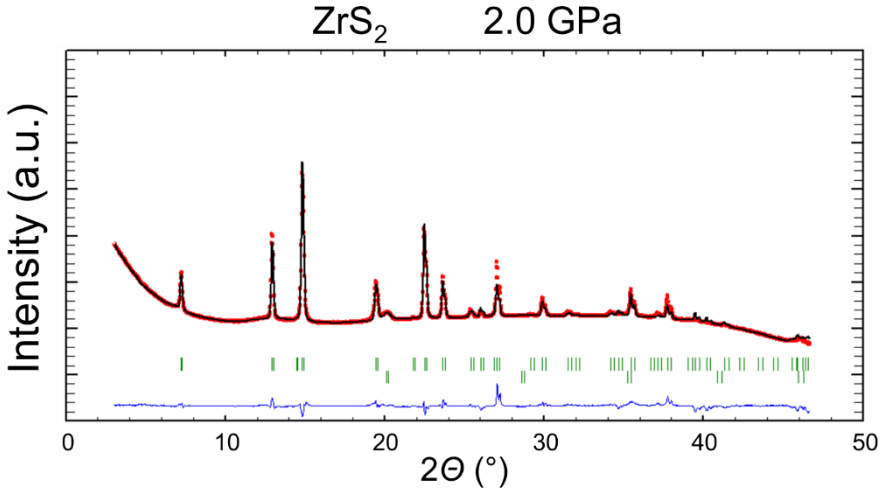
ZrS2 2.0 GPa
Intensity (a.u.)
0
10
20
30
40
50
2Θ (°)

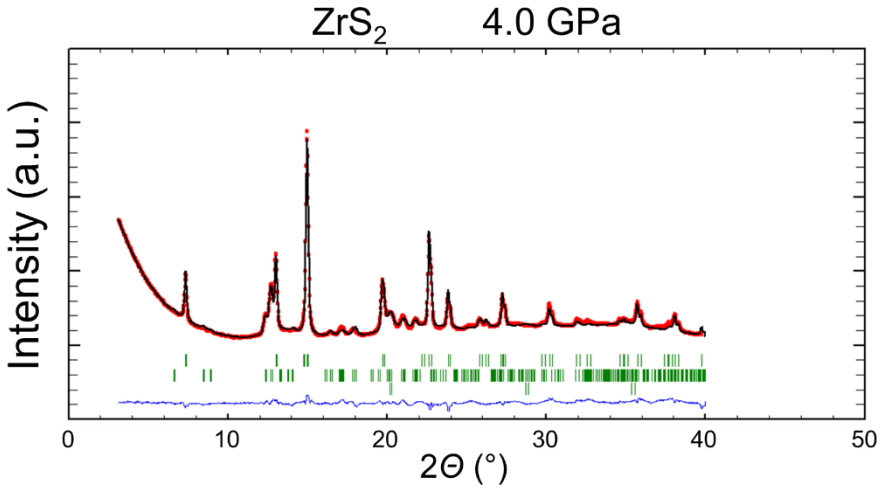
ZrS2 4.0 GPa
Intensity (a.u.)
0
10
20
30
40
50
2Θ (°)

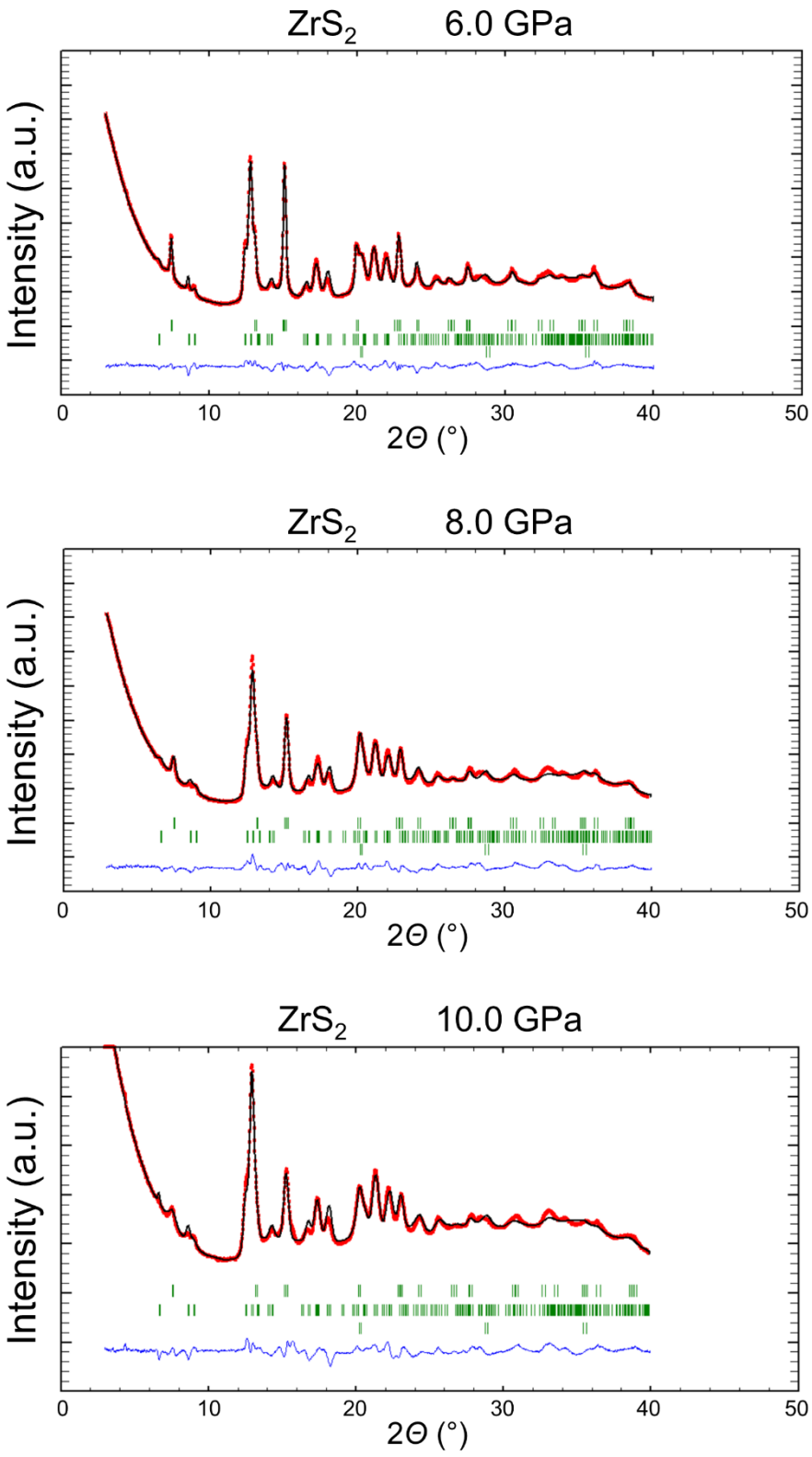

Figure SI 1 Results of the Rietveld refinement from X-ray diffraction analysis (λ_{Mo}) of ZrS_2.

Table X. Results of the Rietveld refinement from X-ray diffraction analysis (λ_{Mo}) of $ZrSe_2$.

Pressure 0.4GPa			
1T-$ZrSe_2$	*P* -3*m1*	R_{Bragg} = 7.72 %	Fract. (%) = 98 (8)
a = b = 3.7656 (2) Å	*c* = 6.0953 (30) Å		
V = 74.854 (37) Å^3			
Strain Parameters (for profile only, large esd)			
S_{400}=1.16 (34), S_{004}=5.76 (4.31), S_{112}=3.32 (4.50)			
Fe	*I m3m*	R_{Bragg} = 6.65 %	Fract. (%) = 2 (2)
a = 2.8756 (8) Å			
V = 23.779 (11) Å^3			
Pressure 1.7GPa			
1T-$ZrSe_2$	*P* -3*m1*	R_{Bragg} = 8.28 %	Fract. (%) = 98 (10)
a = b = 3.7335 (13) Å	*c* = 6.0164 (71) Å		
V = 72.629 (92) Å^3			
Strain Parameters (for profile only, large esd)			
S_{400}= 0.51 (18), S_{004}= 5.68 (4.33), S_{112}= 3.19 (4.30)			
Fe	*I m3m*	R_{Bragg} = 7.07%	Fract. (%) = 2 (2)
a = 2.8486 (10) Å			
V = 23.114 (14) Å^3			
Pressure 3.3GPa			
1T-$ZrSe_2$	*P* -3*m1*	R_{Bragg} = 10.5 %	Fract. (%) = 99 (7)
a = b = 3.7213 (2) Å	*c* = 5.8494 (24) Å		
V = 70.150 (29) Å^3			
Strain Parameters (for profile only, large esd)			
S_{400}= 1.20 (27), S_{004}= 4.11 (3.13), S_{112}= 0.22 (3.07)			
Fe	*I m3m*	R_{Bragg} = 4.07 %	Fract. (%) = 1 (3)
a = 2.8215 (56) Å			
V = 22.462 (8) Å^3			
Pressure 5.2GPa			

1T-$ZrSe_2$	*P* -3*m1*	R_{Bragg} = 14.4 %	Fract. (%) = 99 (6)
a = b = 3.6909 (2) Å	*c* = 5.7716 (27) Å		
V = 68.090 (33) Å^3			
Strain Parameters (for profile only, large esd)			
S_{400}= 15.32 (2.45), S_{004}= 55.78 (14.19), S_{112}=0			
Fe	*I m3m*	R_{Bragg} = 3.90 %	Fract. (%) = 1(1)
a = 2.7942 (9) Å			
V = 21.817 (12) Å^3			
Pressure 7.4GPa			
1T-$ZrSe_2$	*P* -3*m1*	R_{Bragg} = 10.2 %	Fract. (%) = 58 (5)
a = b = 3.6473 (9) Å	*c* = 5.7208 (1) Å		
V = 65.907 (24) Å^3			
Strain Parameters (for profile only, large esd)			
NR			
HP-$ZrSe_2$	*I mmm*	R_{Bragg} = 14.3 %	Fract. (%) = 41 (2)
a = 3.6097 (20) Å	*b* = 5.3843 (82) Å	*c* = 12.1040 (103) Å	
V = 235.252 (432) Å^3			
Strain Parameters (for profile only, large esd)			
S_{400}= 6.98(7.71), S_{040}= 21.10 (31.36), S_{004}= 1.43 (1.44), S_{220}= 10.68 (72.44), S_{202}=0, S_{022}=0			
Fe	*I m3m*	R_{Bragg} = 3.16 %	Fract. (%) = 1(1)
a = 2.7664 (0.0032) Å			
V = 21.171 (42) Å^3			
Pressure 9.5GPa			
1T-$ZrSe_2$	*P* -3*m1*	R_{Bragg} = 13.3 %	Fract. (%) = 39 (5)
a = b = 3.6189 (16) Å	*c* = 5.7208 (2) Å		
V = 64.886 (41) Å^3			
Strain Parameters			
NR			
HP-$ZrSe_2$	*I mmm*	R_{Bragg} = 13.9 %	Fract. (%) = 61 (8)
a = 3.5824 (21) Å	*b* = 5.3699 (84) Å	*c* = 12.0613 (233) Å	
V = 232.023 (592) Å^3			
Strain Parameters (for profile only, large esd)			
S_{400}= 0.48 (41), S_{040}= 1.03 (1.55), S_{004}= 0.09 (7), S_{220}= 1.55 (3.81), S_{202}= 0, S_{022}=0			
Fe	*I m3m*	R_{Bragg} = 0.5 %	Fract. (%) = 0 (1)
a = 2.7413 (497) Å			

V = 20.599 (647) Å^3

Pressure 11.5GPa			
1T-ZrS_2	*P* -3*m1*	R_{Bragg} = 17.1 %	Fract. (%) = 19(3)
a = b = 3.6307 (22) Å	*c* = 5.6089 (501) Å		
V = 64.031 (574) Å^3			
Strain Parameters			
NR			
HP-ZrS_2	*I mmm*	R_{Bragg} = 15.4 %	Fract. (%) = 81 (10)
a = 3.5894 (239) Å	*b* = 5.4119 (111) Å	*c* = 12.0219 (116) Å	
V = 233.527 (552) Å^3			
Strain Parameters (for profile only, large esd)			
S_{400}= 1.09(0.74), S_{040}= 2.03 (2.72), S_{004}= 0.07 (0.08), S_{220}= NR, S_{202}= 0.67 (0.68), S_{022}=0			
Fe			
not refined	*I m3m*	R_{Bragg} = NR	Fract. (%) = NR
(too much overlap)			
a = NR			
V = NR			

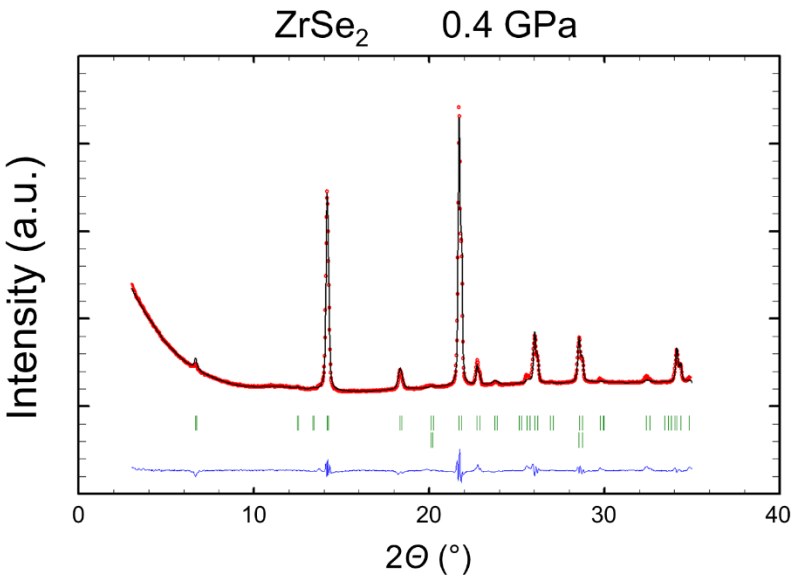
ZrSe2 0.4 GPa
Intensity (a.u.)
0
10
20
30
40
2Θ (°)

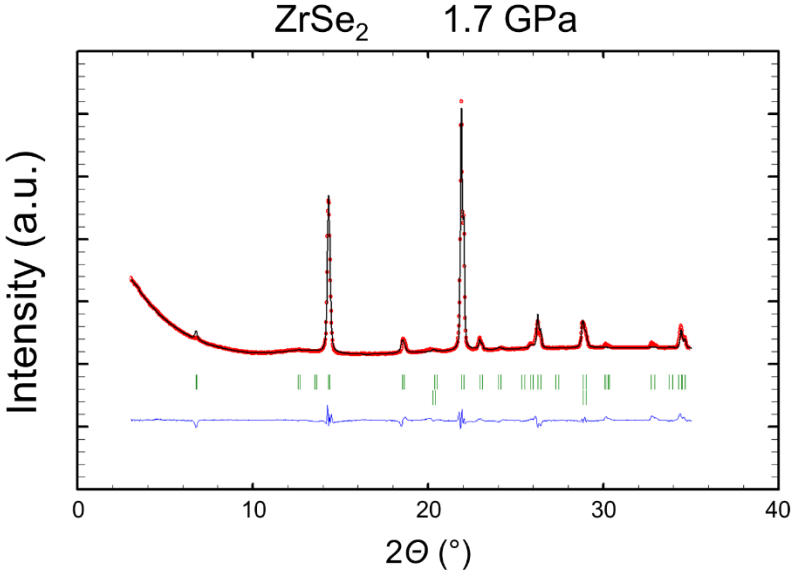
ZrSe2 1.7 GPa
Intensity (a.u.)
0
10
20
30
40
2Θ (°)

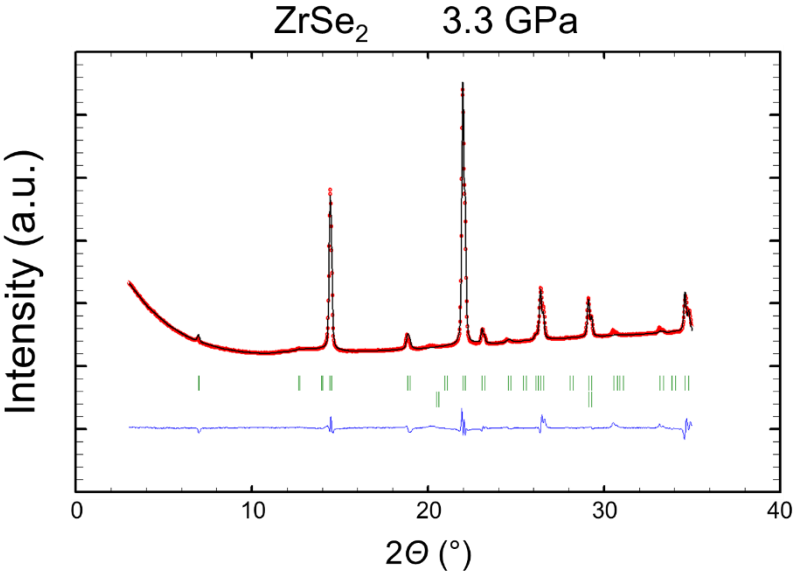
ZrSe2 3.3 GPa
Intensity (a.u.)
0
10
20
30
40
2Θ (°)

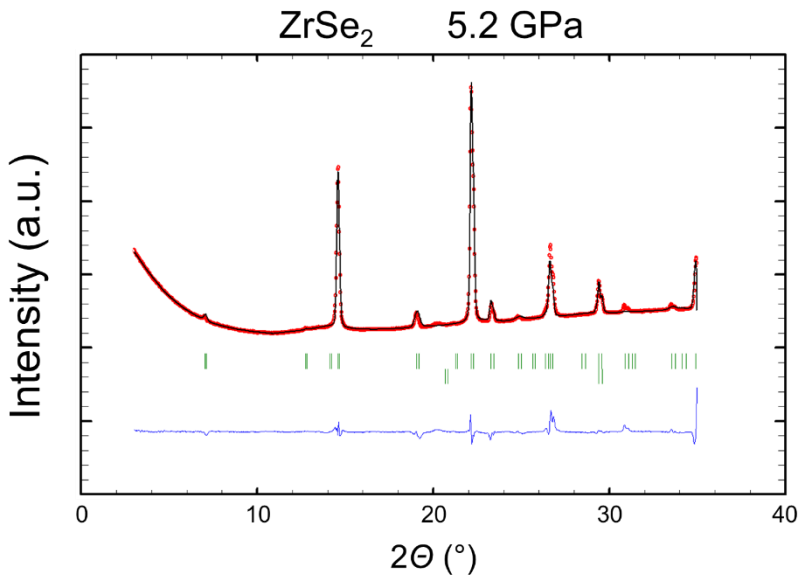
ZrSe2 5.2 GPa
Intensity (a.u.)
0
10
20
30
40
2Θ (°)

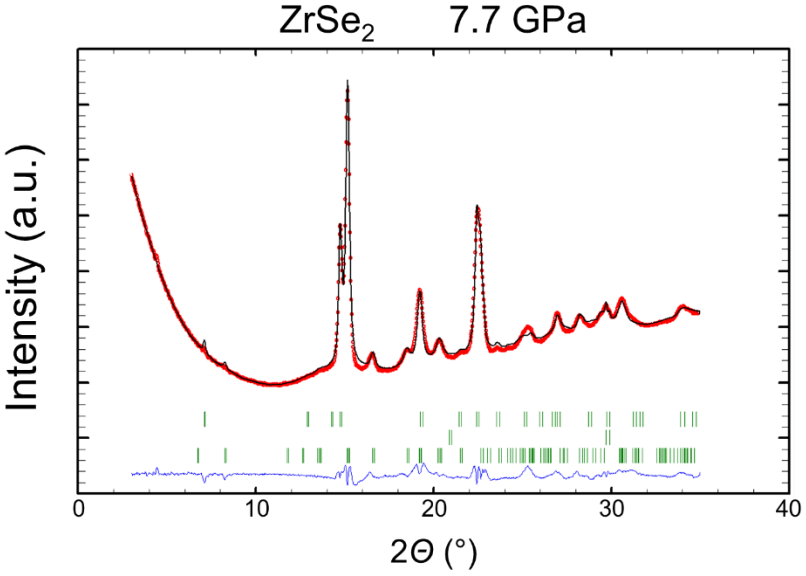
ZrSe2 7.7 GPa
Intensity (a.u.)
0
10
20
30
40
2Θ (°)

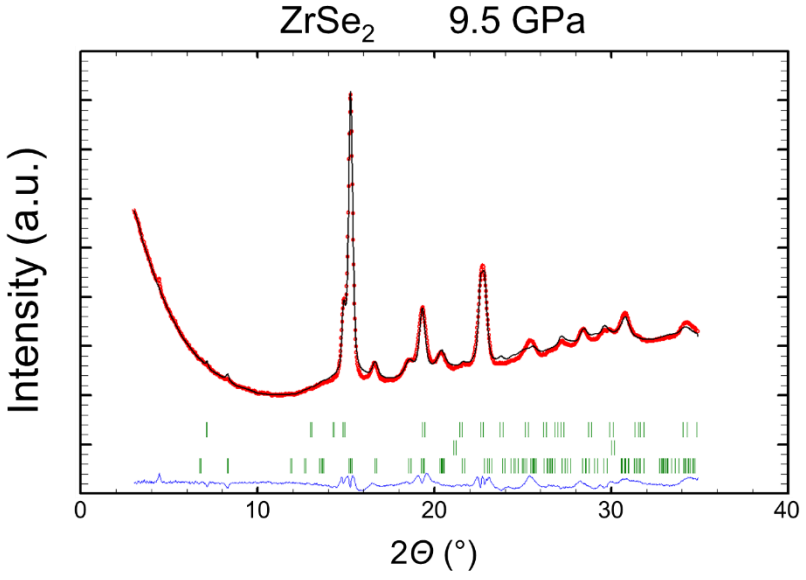
ZrSe2 9.5 GPa
Intensity (a.u.)
0
10
20
30
40
2Θ (°)

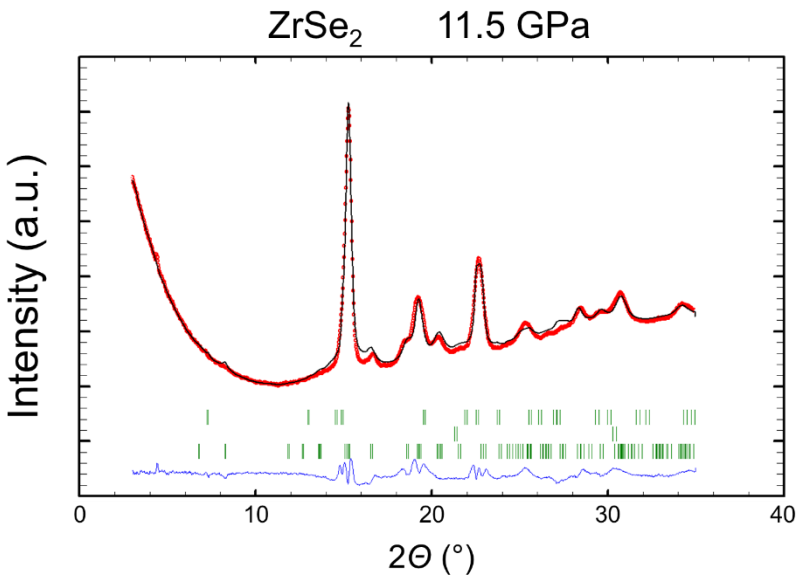

Figure SI 2 Results of the Rietveld refinement from X-ray diffraction analysis (λ_{Mo}) of ZrS_2.

Pressure - Strain relation

Given the experimental X-ray diffraction (XRD) data, recorded during high-pressure experiments, it is possible to compute the change in unit cell parameters of the 1T-phases of ZrS_2 and $ZrSe_2$. The data were used to compute the pressure – strain relation for the material.

The engineering strain (in percentage) applied to the material is computed as:

$$\varepsilon_a(P) = \frac{a(P)-a(0)}{a(0)} \cdot 100 \quad (1)$$

Where $a(0)$ and $a(P)$ are the same lattice parameter at ambient and pressure P respectively. Given the hydrostatic conditions of the experiment, only the three diagonal component of the strain tensor are non-zero: ε_a, ε_b and ε_c. Because of the hexagonal lattice symmetry (P-3m1),

$$\varepsilon_a = \varepsilon_b. \quad (2)$$

As a reference, strain is considered positive when tensile and negative when compressive. In the case of our high-pressure experiments, ε is negative as only compressive deformation is produced. In Figure SI 1, we report the computed values, extracted from high-pressure powder XRD for 1T-ZrS_2 and 1T-$ZrSe_2$. As a comparison, Figure SI 2 shows the compressibility as function of pressure for the semiconducting 2H polytypes (MoS_2, WS_2 and WSe_2), computed from published results [11,12,13].

From our results the 1T polytypes appear to have a much higher compressibility than the 2H polytypes. In comparison, at 10 GPa, in-plane strain are ε_a=3.6% and ε_a=2.2% for 1T and 2H respectively. For both materials, the out-of-plane compressibility is much higher than the in-plane one, as one would expect considering the much weaker van der Waals interaction.

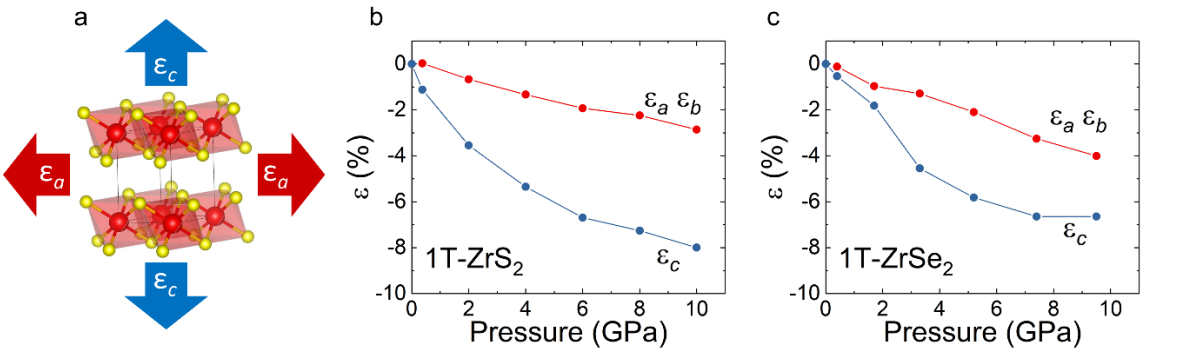

Figure SI 3. a) 1T-ZrX_2 unit cell. The arrows point in the direction of positive strains (tensile) along 2 principal directions, ε_a is in-plane and ε_c is out-of-plane. **b**) Experimentally determined pressure-strain relation for 1T-ZrS_2. **c**) Experimentally determined pressure-strain relation for 1T-$ZrSe_2$.

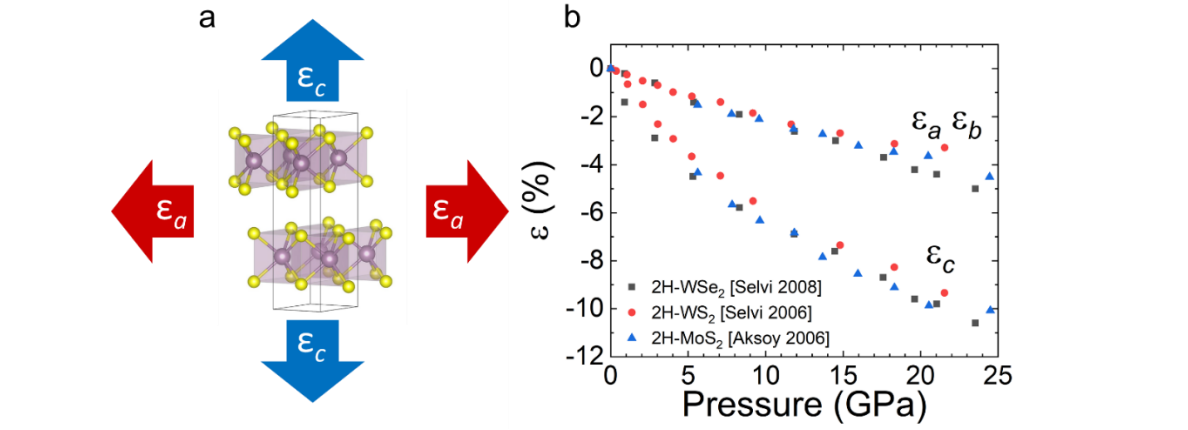

Figure SI 4. a) 2H-MeX_2 unit cell. The arrows point in the direction of positive strains (tensile) along 2 principal directions. **b**) Experimentally determined pressure-strain relation for 2H-MoS_2, 2H-WS_2 and 2H-WSe_2.

High-pressure Raman scattering

Here we show the Raman spectra at each pressure during compression and decompression.

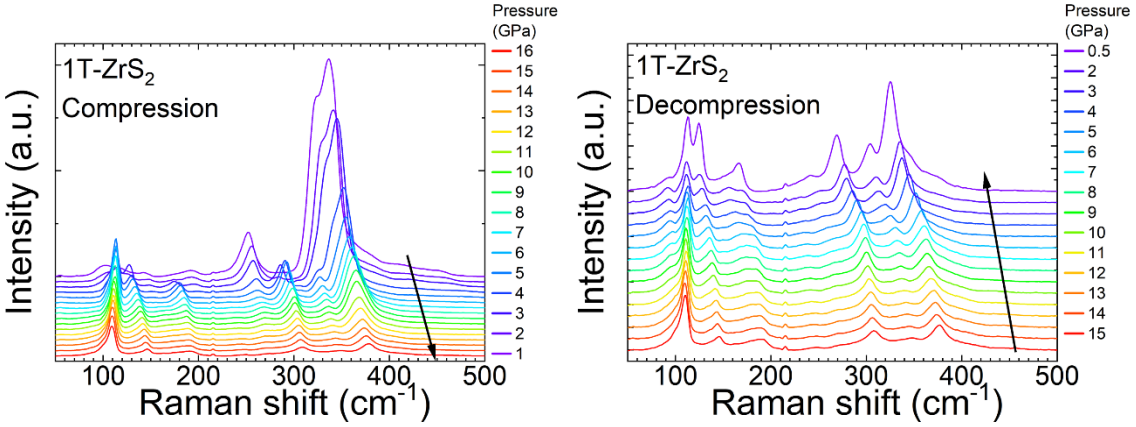

Figure SI 5. Raman spectra of ZrS_2 collected during compression and decompression. All curves are shifted vertically by an equal amount.

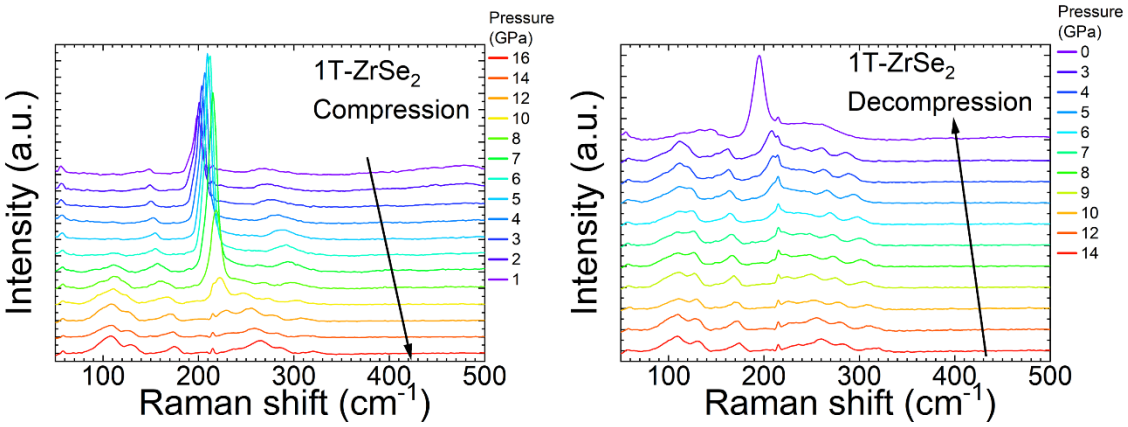

Figure SI 6. Raman spectra of $ZrSe_2$ collected during compression and decompression. All curves are shifted vertically by an equal amount.

Band gap estimation from optical transmittance

Values of the optical band gap as a function of pressure were estimated from the optical transmittance data. As all semiconducting phases have an indirect band gap, we used the same empirical model for all data points. After computing the absorption coefficient (α) from the experimental data, we estimated the indirect band gap E_g via linear extrapolations of $(h\vartheta\alpha)^{1/2}$. Representative fitting are shown in Figure SI. 7.

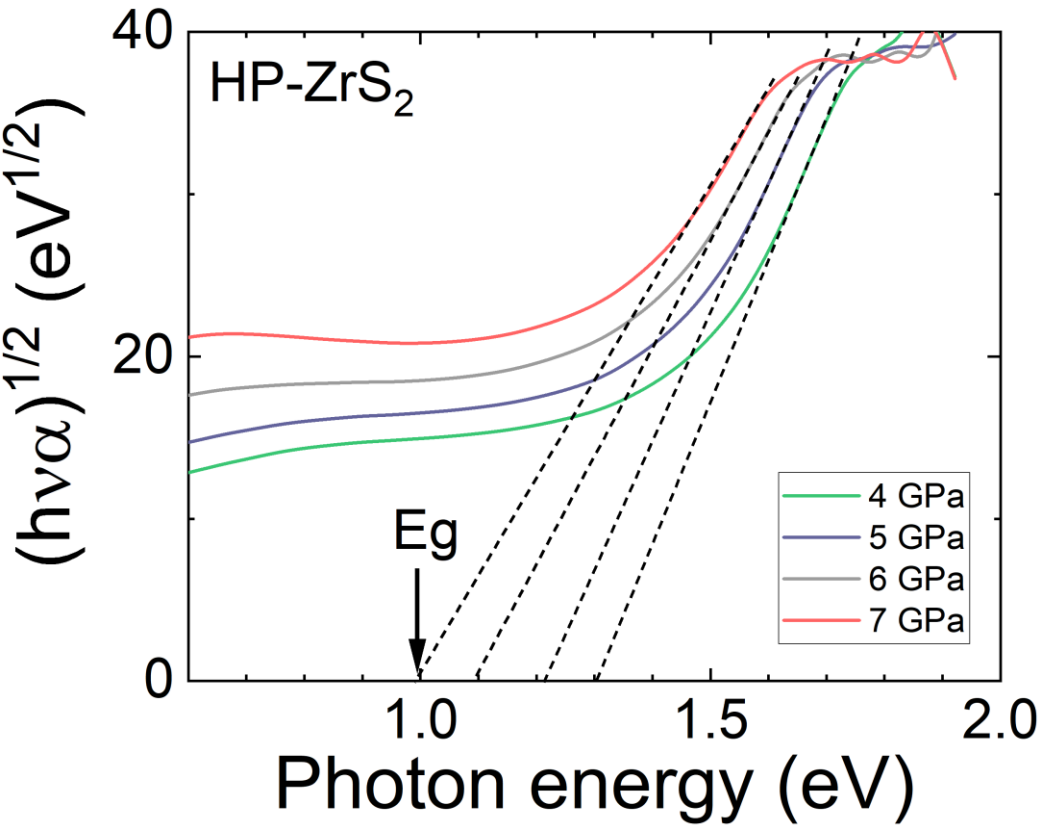

Figure SI 7. Representative extrapolation of the indirect band gap for the high-pressure phase of ZrS_2 (HP-ZrS_2) at different pressures.

DFT band structures calculations

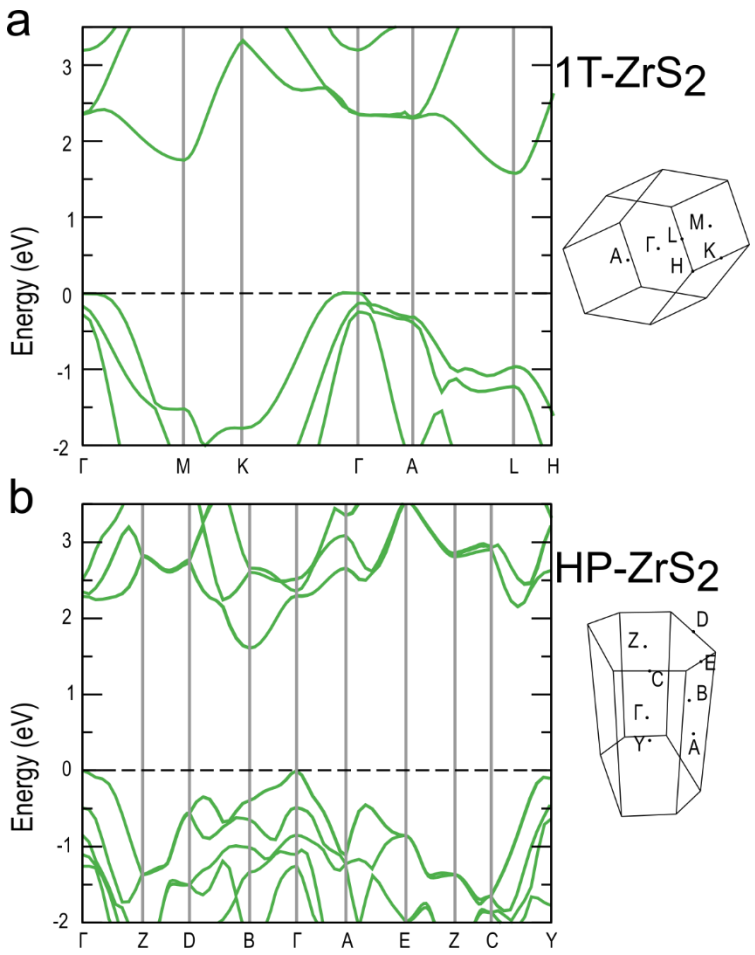

Figure SI 8. Electronic band structure of the (a) low-pressure (0 GPa) and (b) high-pressure (6 GPa) crystalline phases of ZrS_2, together with the high-symmetry points in the corresponding first Brillouin zones.

References

[1] Livache, C. et al. Effect of Pressure on Interband and Intraband Transition of Mercury Chalcogenide Quantum Dots. J. Phys. Chem. C. 2019, 123, 13122–13130.

[2] Celeste, A., Borondics, F. & Capitani, F. Hydrostaticity of pressure-transmitting media for high pressure infrared spectroscopy. High Press. Res. 2019, 39, 608–618.

[3] Reijnders, Anjan A., et al. Fourier analysis of the IR response of van der Waals materials. arXiv preprint arXiv:1407.6713, 2014.

[4] Chervin, J. C., B. Canny, and M. Mancinelli. Ruby-spheres as pressure gauge for optically transparent high pressure cells. Inter. J. of High Pressure Research. 2001, 21.6, 305-314.

[5] Klotz, S., et al. Hydrostatic limits of 11 pressure transmitting media. J. of Physics D: Applied Physics. 2009, 42.7, 075413 1-7.

[6] Joubert, D. From ultrasoft pseudopotentials to the projector augmented-wave method. Phys. Rev. B - Condens. Matter Mater. Phys. 1999, 59, 1758–1775.

[7] Kresse, G. & Furthmüller, J. Efficient iterative schemes for ab initio total-energy calculations using a plane-wave basis set. Phys. Rev. B - Condens. Matter Mater. Phys. 1996, 54, 11169–11186.

[8] Heyd, J., Scuseria, G. E. & Ernzerhof, M. Hybrid functionals based on a screened Coulomb potential. J. Chem. Phys. 2003, 118, 8207–8215.

[9] Perdew, J. P., Burke, K. & Ernzerhof, M. Generalized gradient approximation made simple. Phys. Rev. Lett. 1996, 77, 3865–3868.

[10] Rodríguez-Carvajal, Juan. "Recent advances in magnetic structure determination by neutron powder diffraction." *Physica B.* **1993**, 192.1-2: 55-69.

[11] Aksoy, R. et al. X-ray diffraction study of molybdenum disulfide to 38.8 GPa. *J. Phys. Chem. Solids.* **2006**, 67, 1914–1917.

[12] Selvi, E., Ma, Y., Aksoy, R., Ertas, A. & White, A. High pressure X-ray diffraction study of tungsten disulfide. *J. Phys. Chem. Solids*. **2006**, 67, 2183–2186.

[13] Selvi, E., Aksoy, R., Knudson, R. & Ma, Y. High-pressure X-ray diffraction study of tungsten diselenide. *J. Phys. Chem. Solids*. **2008**, 69, 2311–2314.